Check for updates

Geophysical Research Letters

RESEARCH LETTER
10.1029/2025GL118546

Wind-Driven Coastal Polynya Variability Drives Decadal Ice-Shelf Melt Variability in the Amundsen Sea

Michael Haigh[1], **Paul R. Holland**[1], **Thomas Caton Harrison**[1], **and Pierre Dutrieux**[1]

[1]British Antarctic Survey, Cambridge, UK

Key Points:

- Atmospheric forcing perturbation experiments unveil the drivers of decadal ice-ocean variability in the Amundsen Sea
- Shelf-break undercurrent and ice-shelf melt variability are driven by variable sea-ice freshwater fluxes in wind-driven polynyas
- Feedbacks from ice-shelf melting further enhance undercurrent and melt anomalies

Supporting Information:

Supporting Information may be found in the online version of this article.

Correspondence to:

M. Haigh,
michai@bas.ac.uk

Citation:

Haigh, M., Holland, P. R., Harrison, T. C., & Dutrieux, P. (2026). Wind-driven coastal polynya variability drives decadal ice-shelf melt variability in the Amundsen Sea. *Geophysical Research Letters*, *53*, e2025GL118546. https://doi.org/10.1029/2025GL118546

Received 31 JUL 2025
Accepted 12 JAN 2026

Author Contributions:

Conceptualization: Michael Haigh
Data curation: Michael Haigh, Pierre Dutrieux
Formal analysis: Michael Haigh, Thomas Caton Harrison
Investigation: Michael Haigh, Thomas Caton Harrison
Methodology: Michael Haigh, Pierre Dutrieux
Resources: Pierre Dutrieux
Software: Michael Haigh
Validation: Michael Haigh, Thomas Caton Harrison, Pierre Dutrieux
Visualization: Michael Haigh
Writing – original draft: Michael Haigh
Writing – review & editing: Thomas Caton Harrison, Pierre Dutrieux

© 2026. The Author(s).
This is an open access article under the terms of the Creative Commons Attribution License, which permits use, distribution and reproduction in any medium, provided the original work is properly cited.

Abstract The ice shelves in the Amundsen Sea are being melted rapidly by warm Circumpolar Deep Water (CDW), causing sea-level rise. Ice-shelf melt variability is controlled by the speed of a shelf-break undercurrent which transports CDW onto the continental shelf. We study decadal variability of the undercurrent and ice-shelf melting using new regional ice-ocean model perturbation experiments. The perturbation experiments suggest that the undercurrent decadal variability is controlled by variable coastal sea-ice freshwater fluxes, these driven by winds mechanically opening and closing coastal polynyas. With the perturbation experiments we also quantify a positive feedback mechanism between the undercurrent and ice-shelf melting which is responsible for 25% of their decadal variability.

Plain Language Summary Glaciers flowing into the Amundsen Sea, West Antarctica are being melting rapidly by warm ocean waters, contributing to global sea-level rise. A deep ocean current is responsible for delivering this warm water to the glacial ice. On decadal timescales the speed of this current varies, which causes the rate of ice melting to vary. In our study model experiments suggest that the variability in the speed of the current is controlled by changes in the formation of sea ice. These experiments also suggest that changes in the sea-ice formation are caused by variations in the winds near the Amundsen Sea coast.

1. Introduction

The ice streams flowing into the Amundsen Sea, West Antarctica, are losing mass faster than most others about the continent (Mouginot et al., 2014; Rignot et al., 2014), contributing to global sea-level rise (Shepherd et al., 2018). The ice loss is caused by basal melting of the downstream ice shelves by warm Circumpolar Deep Water (CDW). Concerns surrounding this region are elevated by modeling studies (Jourdain et al., 2022; Naughten et al., 2023) which project an anthropogenically forced acceleration of ice-shelf melting over the coming century.

Ice-shelf melt variability is dynamically tied to the Amundsen Sea undercurrent, a warm current carrying CDW that flows eastward along the continental slope. Observations show this current turns onto the continental shelf at bathymetric troughs that intersect the shelf break (Assmann et al., 2013; Walker et al., 2007, 2013), simultaneously transporting CDW onto the continental shelf. This CDW is eventually advected towards the ice shelves where it drives rapid melting. Through this process, variability in the undercurrent speed controls ice-shelf melt variability (Dotto et al., 2019, 2020; Jenkins et al., 2016).

Processes controlling undercurrent variability are timescale-dependent. On monthly-yearly timescales the undercurrent speed is controlled by shelf-break winds (Assmann et al., 2013; Azaneu et al., 2023) which barotropically accelerate the surface and deep flow alike. On centennial timescales trends in the undercurrent are caused by trends in atmospheric thermodynamically forced changes to sea-ice formation (Turner et al., 2025). This study aims to provide clarity on important processes acting on intermediate decadal timescales (Dutrieux et al., 2014; Jenkins et al., 2018).

Silvano et al. (2022) presented model output showing that the undercurrent decadal variability does not follow the shelf-break winds, countering understanding (Holland et al., 2019, e.g.) at the time. Haigh and Holland (2024) showed that in the same model sea-ice freshwater fluxes on and off the continental shelf alter the cross-slope density gradient and baroclinically accelerate and decelerate the undercurrent. However, these studies were based on just a single simulation; in this study we develop a suite of perturbation experiments to reach a stronger mechanistic understanding of the modeled decadal variability. We find the decadal variability is predominantly controlled by winds affecting coastal sea-ice freshwater fluxes and in turn the shelf-break undercurrent.

19448007, 2026, 2, Downloaded from https://agupubs.onlinelibrary.wiley.com/doi/10.1029/2025GL118546 by British Antarctic Survey, Wiley Online Library on [22/01/2026]. See the Terms and Conditions (https://onlinelibrary.wiley.com/terms-and-conditions) on Wiley Online Library for rules of use; OA articles are governed by the applicable Creative Commons License

2. Methods

2.1. Amundsen Sea Regional Model

We use a 0.1° regional configuration of MITgcm including ocean, sea-ice and ice-shelf components. The model uses climatological boundary conditions and is forced using six-hourly ERA5 (Hersbach et al., 2020) 10-m winds, surface longwave and shortwave radiation, 2-m air temperature, 2-m specific humidity, precipitation and atmospheric pressure. We use ERA5 as it is considered one of the most reliable reanlyses for Antarctica (Gossart et al., 2019; Tetzner et al., 2019). The model is spun up using the 1979–2002 forcing, after which the model is restarted and run from 1979 to 2021 with monthly output.

An exception in the forcing regime is the year 1996 for which we use ERA-Interim since an error was identified in ERA5 for 1996 (Figure S1 in Supporting Information S1) which affects the simulation of Silvano et al. (2022) and Haigh and Holland (2024). This error consists of an unrealistically strong, semi-permanent low-pressure center over the deep ocean. ERA-Interim is the ideal replacement for 1996 given high correlations outside of 1996 with ERA5.

Our model has previously been verified (Dotto et al., 2019, 2020; Naughten et al., 2022), but we conduct further verifications utilizing an updated Pine Island Glacier mooring record (Figure S2 in Supporting Information S1). The model reproduces the local 0°C isotherm depth (a measure pertinent for ice-shelf melting), but is affected by brief, localized convective events not present in observations. While these convective events can briefly impact local ice-shelf melt rates, our conclusions are not affected since these are based on larger-scale spatial and temporal averages. For further details we refer the reader to the Supporting Information and to Naughten et al. (2022) who conducted a detailed model validation of temperature/salinity profiles, ice-shelf melt rates, and sea-ice concentration.

2.2. Perturbation Experiments

To examine drivers of decadal variability we develop perturbation experiments in which individual atmospheric forcing variables either remain their default 1979–2021 values or are fixed to a repeating four-year cycle. For the repeating cycle the year 1991 is repeated three times followed by the year 1992 once (for leap years). We use the years 1991/1992 for the perturbation experiments since during this period the major climate indices El Niño-Southern Oscillation and the Southern Annular Mode are in neutral phases (Stewart et al., 2020).

We define five simulations. ALL: the reference simulation with all atmospheric variables varying as normal. WINDS: winds varying as normal, with all other variables fixed to the repeating 1991/1992 cycle. THERMO: winds fixed to the repeating 1991/1992 cycle, with all other variables varying as normal. NONE: all atmospheric variables fixed to the 1991/1992 cycle. ALL NO FEEDBACK: ice-shelf meltwater fluxes fixed to the 1991–1992 time-mean computed in ALL. To confirm the suitability of 1991/1992, NONE simulations were conducted for all 11 possible year/leap year pairs between 1979 and 2021. Timeseries of the resulting undercurrent and ice-shelf melting (Figure S3 in Supporting Information S1) show that using the years 1991/1992 leads to a simulation with a steady state within the variability of ALL.

With ALL, WINDS, THERMO and NONE, we can determine whether Amundsen Sea decadal variability is driven by atmospheric winds or thermodynamics. The wind variables appear in both the surface stresses and the turbulent heat and moisture fluxes. To ensure WINDS has no decadal variability in the atmospheric thermodynamic forcing, the repeating 1991/1992 winds are used in the computation of the turbulent heat fluxes. Likewise, for consistency in THERMO, the fully varying winds are used in the computation of the turbulent heat fluxes.

ALL NO FEEDBACK is used to determine the importance of feedbacks between ice-shelf melting and the undercurrent. This is motivated by studies (Haigh et al., 2023; Moorman et al., 2020; Si et al., 2023) which have highlighted the role of ice-shelf melting in maintaining the on-shelf density structure. In ALL NO FEEDBACK we diagnose the time-varying ice-shelf melting as usual, but instead input into the ocean constant ice-shelf heat and salt fluxes equal to the 1991–1992 ALL time-mean.

2.3. Undercurrent Definition

We define the undercurrent following Haigh and Holland (2024). For each longitude along the 1000 m shelf-break isobath the along-slope flow beneath the 1028 kg m^{-3} isopycnal and above 800 m depth is averaged over a

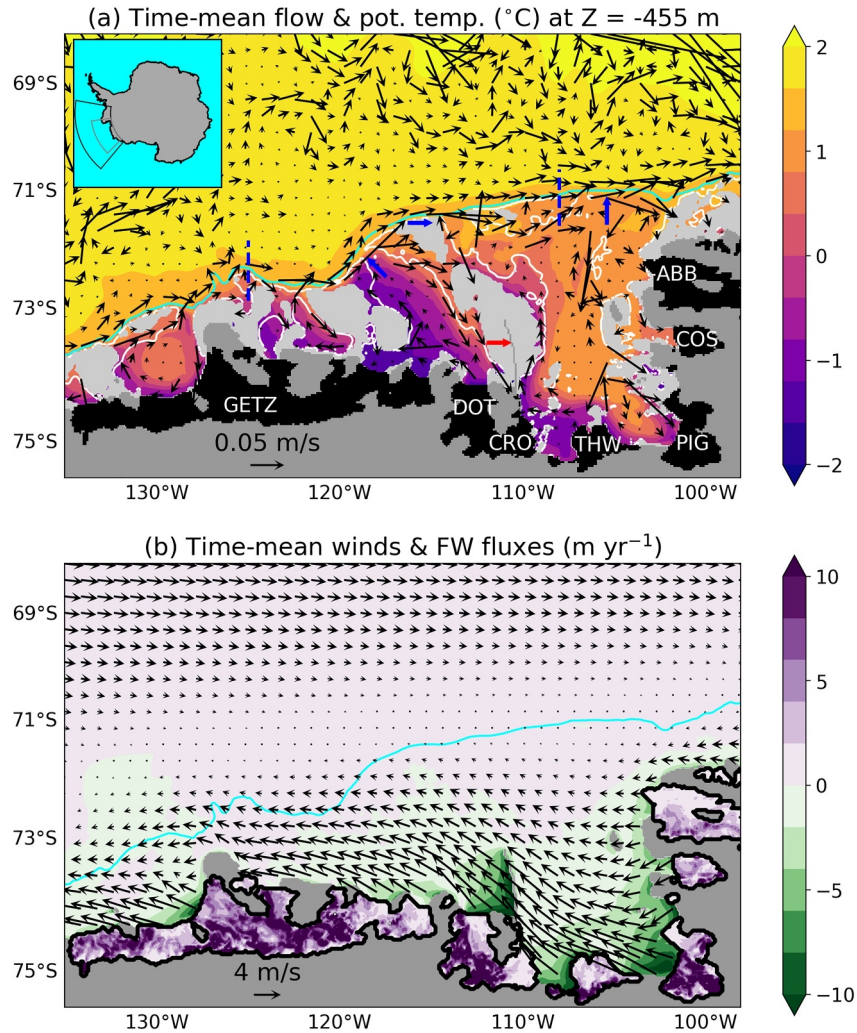

Figure 1. (a) Modeled time-mean flow (arrows) and potential temperature (color) at 450 m depth. Light gray masking represents bathymetry shallower than 450 m, dark gray masking represents land/ice sheets and black masking represents ice shelves. Blue arrows indicate the Dotson-Getz and Pine Island-Thwaites West/East troughs. The red arrow indicates Bear Ridge. Inset: map showing model domain (black box) and subregion shown in this figure (gray box). (b) Time-mean winds (arrows) and sea-ice and ice-shelf freshwater fluxes (color). Positive freshwater fluxes correspond to ocean freshening. The ice shelves are outlined by the thick black contour. The cyan (white) contour represents the 1000 m (500 m) isobath.

meridional range of seven grid points centered on the isobath. The undercurrent speed at each longitude is then defined as the maximum, evaluated over depth, of these meridionally averaged values. We then zonally average the undercurrent speed along the 1000 m isobath between 125°W and 108°W, the undercurrent longitudes of interest. Dotson-Getz and Pine Island-Thwaites West troughs (Figure 1a) are excluded from this zonal average as these are locations at which the undercurrent turns onto the continental shelf. Using alternate undercurrent definitions does not affect our conclusions.

We are also interested in the baroclinicity at the shelf break. We define this as the difference between the eastward undercurrent speed and the surface flow. The surface flow is computed by averaging the along-slope upper-layer velocity over the same lateral area as for the undercurrent.

2.4. Statistical Methods

With an interest in decadal variability, we detrend and apply a 4-year running mean to all presented timeseries. Correlations between timeseries are computed using the Pearson correlation coefficient. Correlation significance is computed using a two-sided Student's *t*-test, with the effective degrees of freedom defined as the number of

19448007, 2026, 2, Downloaded from https://agupubs.onlinelibrary.wiley.com/doi/10.1029/2025GL118546 by British Antarctic Survey, Wiley Online Library on [22/01/2026]. See the Terms and Conditions (https://onlinelibrary.wiley.com/terms-and-conditions) on Wiley Online Library for rules of use; OA articles are governed by the applicable Creative Commons License

19448007, 2026, 2, Downloaded from https://agupubs.onlinelibrary.wiley.com/doi/10.1029/2025GL118546 by British Antarctic Survey, Wiley Online Library on [22/01/2026]. See the Terms and Conditions (https://onlinelibrary.wiley.com/terms-and-conditions) on Wiley Online Library for rules of use; OA articles are governed by the applicable Creative Commons License

time samples divided by twice the e-folding decorrelation timescale. This method allows us to account for the fact that our simulations span only two to three cycles of the decadal variability.

We will present composites which use the shelf-break baroclinicity as the predictor. Depending on the variable of interest, composites will be computed over either (a) periods when baroclinicity is maximum/minimum or (b) periods preceding the maxima/minima. The maxima/minima are defined as time periods when the baroclinicity is at least one standard deviation greater than/less than its mean. For the periods preceding the maxima/minima, averages are evaluated over all times between the maxima/minima and the preceding minima/maxima. Figure S4 in Supporting Information S1 shows the baroclinicity timeseries and periods over which composites are computed.

3. Results

3.1. Time-Mean State

Figure 1a shows the time-mean (1979–2021) flow and potential temperature at 450 m depth from ALL. Consistent with observations (Assmann et al., 2013; Walker et al., 2007, 2013) the undercurrent flows eastward along the continental slope and turns onto the continental shelf on the eastern sides of three bathymetric troughs. As it does so, warm CDW is transported onto the continental shelf and onwards towards the ice shelves where it drives rapid basal melt.

Figure 1b shows the time-mean winds, sea-ice freshwater fluxes and ice-shelf freshwater fluxes, illustrating typical forcing of the Amundsen Sea. The time-mean winds are westward over the continental shelf and eastward over the deep ocean. Despite near-zero time-mean winds over much of the continental slope, the eastward undercurrent arises as a baroclinic flow generated by the pressure gradients in the Antarctic Slope Front (ASF), visible in the temperature gradient across the continental slope (Figure 1a). The ASF is maintained by a combination of (a) easterly wind-driven coastal downwelling that forces isopycnals on the continental shelf downwards, and (b) ice-shelf freshwater fluxes that lighten continental shelf waters relative to deep ocean waters. Turner et al. (2025) also recently showed that the annual pattern of sea-ice formation on the continental shelf and sea-ice melt further north decelerates the time-mean undercurrent by lightening the deep ocean waters relative to the shelf waters.

3.2. Undercurrent and Ice-Shelf Melt Variability

Figure 2a shows timeseries of the along-slope surface flow speed, undercurrent speed, baroclinicity, wind speed and ice-shelf melting from ALL. Ice-shelf melt timeseries are area averages computed over all ice shelves shown in Figure 1, with the western half of Getz ice shelf (west of 125°W) omitted since this part of its cavity is not supplied with CDW by the undercurrent. Variability in the undercurrent does not follow variability in the local winds (Silvano et al., 2022), with these instead weakly anti-correlated on timescales longer than 1 year ($r = -0.32$, $p = 0.32$, for 4-year running mean). Ice-shelf melt variability closely follows the undercurrent ($r = 0.92$, $p < 0.05$), reflecting the role that the undercurrent plays in transporting CDW onto the continental shelf. Figure S5 in Supporting Information S1 shows advection of heat onto the continental shelf is balanced by latent heat from ice-shelf melting, evidence that variability in the on-shelf advection of CDW by the undercurrent is responsible for ice-shelf melt variability. Variability in the baroclinicity follows the undercurrent ($r = 0.90$, $p < 0.05$), but with approximately double the magnitude. This is due to the surface flow variability opposing the undercurrent ($r = -0.75$, $p < 0.05$) and instead following the winds ($r = 0.72$, $p < 0.05$).

Figures 2b–2d shows timeseries of the undercurrent speed, baroclinicity and ice-shelf melting from each perturbation experiment. In WINDS, the undercurrent speed, baroclinicity and ice-shelf melting each have decadal variability similar to ALL, suggesting that wind stresses are the primary driver of the variability. In THERMO, there is weak decadal variability over most of the simulation, aside from after 2015 when there are minima in the undercurrent, baroclinicity and ice-shelf melting, each as strong as in WINDS. NONE features almost no decadal variability. In general, the ice-ocean variability in ALL is not equal to the sum of the variabilities from WINDS and THERMO. This represents a nonlinearity in the physical system that we quantify and discuss in Supporting Information S1 (Figure S7).

ALL NO FEEDBACK has variability similar to but weaker than ALL. The ALL NO FEEDBACK ice-shelf melting has standard deviation approximately 25% smaller than in ALL, and the undercurrent and

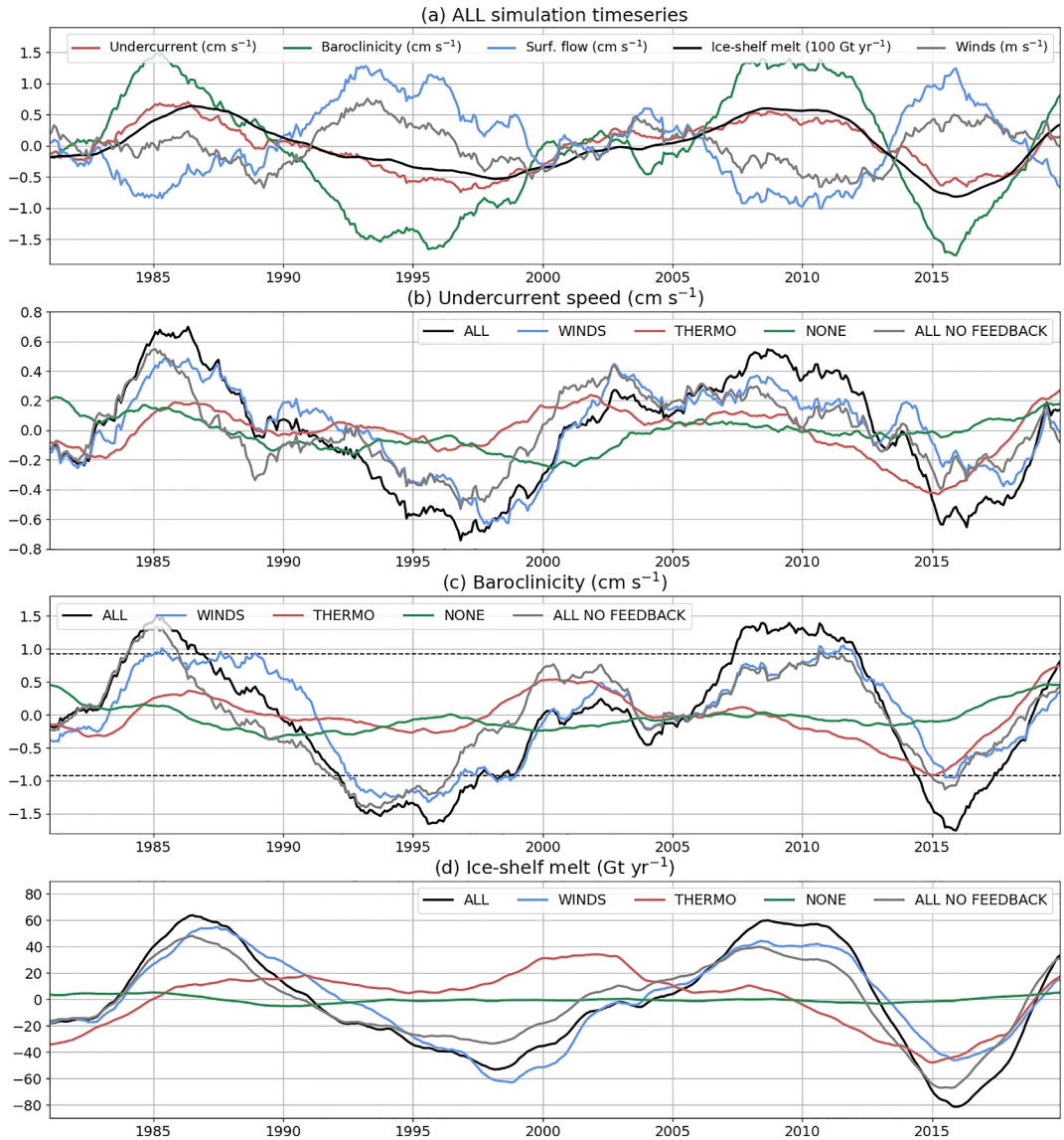

Figure 2. (a) Timeseries of the along-slope undercurrent, baroclinicity, surface flow, wind speed and ice-shelf melting from ALL. Timeseries of the (b) undercurrent, (c) baroclinicity and (d) ice-shelf melting from the five perturbation experiments, ALL, WINDS, THERMO, NONE, and ALL NO FEEDBACK. In (c) the dashed lines represent ±1 standard deviation of the ALL baroclinicity.

baroclinicity have standard deviations approximately 30% smaller than in ALL. This difference quantifies the impact of a positive feedback mechanism between ice-shelf melting and the undercurrent, which we expand on in the next section.

3.3. Cross-Slope Density Variability

Analysis of the cross-slope density further illuminates the drivers of the undercurrent and baroclinicity variability. Figure 3 shows composite anomalies of the cross-slope density and along-slope flow, zonally averaged along the undercurrent pathway, for all five simulations. The composites are averaged over periods when the ALL baroclinicity is one standard deviation above (Figures 3a, 3 c, 3e, 3g, 3i and 3k) and one standard deviation below (Figures 3b, 3 d, 3f, 3h, 3j and 3l) its time mean. In ALL (Figures 3a and 3b), variability in the undercurrent and baroclinicity is a consequence of density variability on the continental shelf altering the cross-slope pressure gradient. The undercurrent is accelerated by negative on-shelf density anomalies and decelerated by positive on-

19448007, 2026, 2, Downloaded from https://agupubs.onlinelibrary.wiley.com/doi/10.1029/2025GL118546 by British Antarctic Survey, Wiley Online Library on [22/01/2026]. See the Terms and Conditions (https://onlinelibrary.wiley.com/terms-and-conditions) on Wiley Online Library for rules of use; OA articles are governed by the applicable Creative Commons License

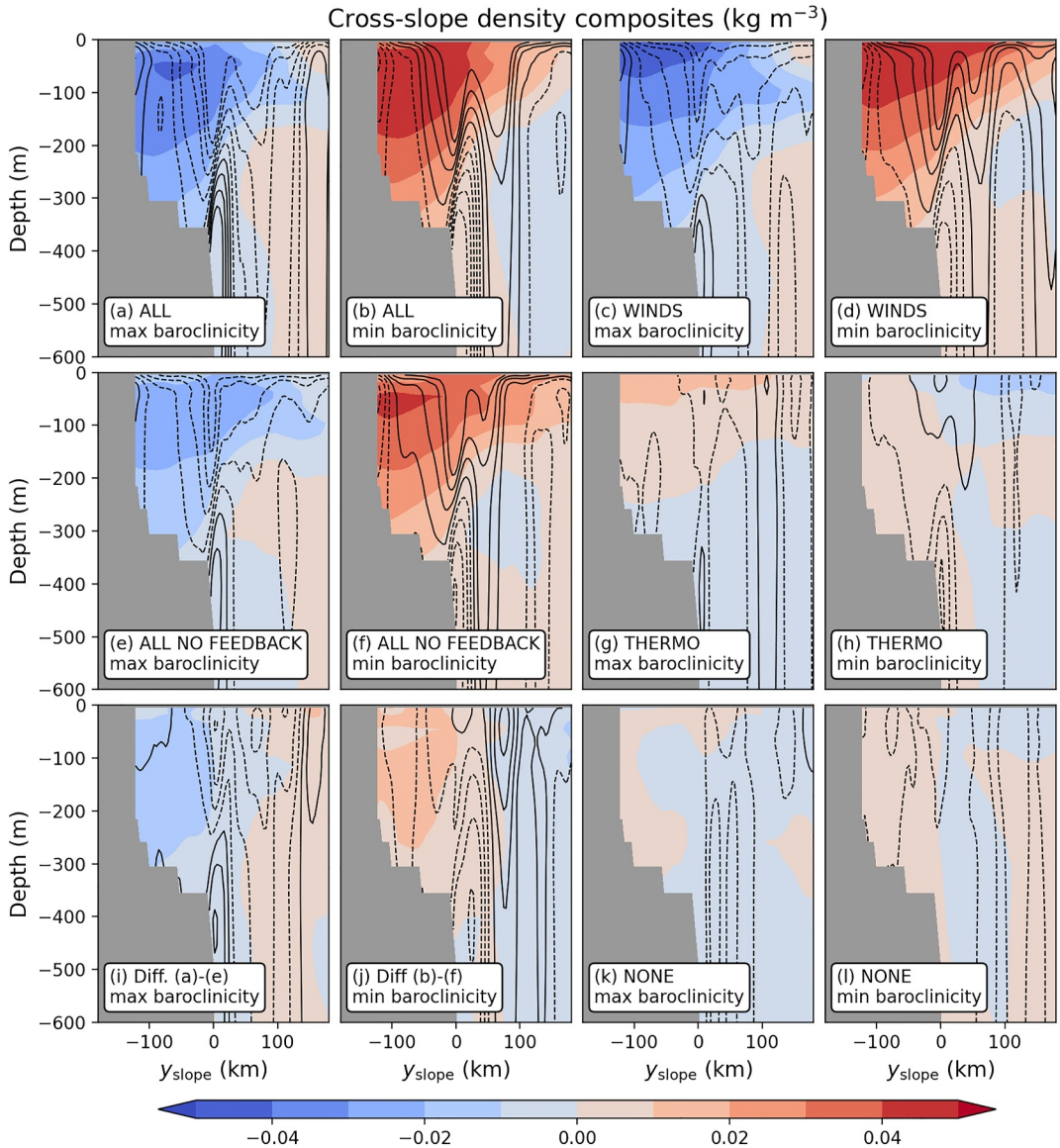

Figure 3. Composite anomalies of the cross-slope density, averaged along the undercurrent pathway, averaged over periods of maximum and minimum baroclinicity. Composites are for (a), (b) ALL (c), (d) WINDS (e), (f) ALL NO FEEDBACK (g), (h) THERMO (i), (j) difference between ALL and ALL NO FEEDBACK (k, l) NONE. Contours represent the along-slope velocity anomalies (1 mm s^{-1} contour interval; dashed are zero and negative). The coordinate y_{slope} is the meridional distance from the 1,000 m continental slope isobath.

shelf density anomalies. This conclusion is similar to Haigh and Holland (2024), where density anomalies both on and off the continental shelf were found to be important. However, the transition to using ERA Interim in 1996, avoiding the ERA5 error, has led to density variability north of the shelf break no longer having a strong signal.

In WINDS (Figures 3c and 3d), the on-shelf density anomalies are similar to those in ALL, consistent with the similarities between the ALL and WINDS undercurrent and baroclinicity timeseries (Figure 2). THERMO (Figures 3g and 3h) and NONE (Figures 3k and 3l) both exhibit weak on-shelf density variability and correspondingly weak undercurrent variability. ALL NO FEEDBACK (Figures 3e and 3f) has density variability similar to but 25% weaker than ALL (comparing maximum and minimum density anomalies). This difference (Figures 3i and 3j) quantifies the feedback of ice-shelf melting back onto the undercurrent: as the ice-shelf melting responds to the undercurrent variability, the resulting ice-shelf meltwater input enhances the on-shelf density anomalies and in turn the undercurrent anomalies. While this feedback between ice-shelf melting and the

19448007, 2026, 2, Downloaded from https://agupubs.onlinelibrary.wiley.com/doi/10.1029/2025GL118546 by British Antarctic Survey, Wiley Online Library on [22/01/2026]. See the Terms and Conditions (https://onlinelibrary.wiley.com/terms-and-conditions) on Wiley Online Library for rules of use; OA articles are governed by the applicable Creative Commons License

19448007, 2026, 2, Downloaded from https://agupubs.onlinelibrary.wiley.com/doi/10.1029/2025GL118546 by British Antarctic Survey, Wiley Online Library on [22/01/2026]. See the Terms and Conditions (https://onlinelibrary.wiley.com/terms-and-conditions) on Wiley Online Library for rules of use; OA articles are governed by the applicable Creative Commons License

undercurrent enhances anomalies in both, the initial driver of on-shelf density and undercurrent variability remains to be determined.

3.4. Drivers of Variability

Motivated by Haigh and Holland (2024), we consider sea-ice freshwater fluxes as the potential driver of the variability. Figures 4a–4h shows composites of the sea-ice freshwater flux for ALL, WINDS, THERMO and NONE. These composites are computed by averaging over time preceding the maxima and minima in the baroclinicity (see Figure S4 in Supporting Information S1). Figures 4a and 4b also shows composites of the winds—these are the same for ALL and WINDS, but THERMO and NONE have no decadal variability in the winds.

In ALL (Figures 4a and 4b), periods of maximum baroclinicity/fast undercurrent are preceded by on-shelf freshening anomalies due to reduced sea-ice formation. Periods of minimum baroclinicity/slow undercurrent are preceded by on-shelf sea-ice salinification (negative) anomalies from increased sea-ice formation. The wind composites show that the reduced sea-ice formation preceding baroclinicity maxima is caused by wind anomalies directed south-eastwards towards the coast which close coastal polynyas (Macdonald et al., 2023; O'Connor et al., 2025). The increase in sea-ice formation preceding baroclinicity minima is caused by wind anomalies directed north-westwards away from the coast which open coastal polynyas. The modeled sea-ice formation variability correlates ($r = 0.40$, $p = 0.17$) with estimates from remote sensing (Figure S8 in Supporting Information S1), with uncertainties in these estimates likely weakening this correlation (Nakata et al., 2021).

The WINDS (Figures 4c and 4d) sea-ice freshwater flux composites are similar to those from ALL, but are marginally weaker, in particular for the periods preceding baroclinicity minima. THERMO and NONE exhibit little variability in the sea-ice freshwater fluxes, leading to little variability in the undercurrent and ice-shelf melting.

The sea-ice freshwater flux composites suggest that freshwater fluxes preceding baroclinicity maxima/minima drive the baroclinicity and undercurrent variability. That is, integrated over time the freshwater flux anomalies produce on-shelf density anomalies (Figure 3) that baroclinically accelerate and decelerate the undercurrent. To illustrate this further, Figure 4i shows timeseries of the time-integrated coastal sea-ice freshwater flux for ALL, WINDS, THERMO and NONE. The coastal area of integration is shown in Figure 4g. Also plotted in Figure 4i is the ALL baroclinicity timeseries for comparison. The ALL sea-ice freshwater flux timeseries follows the ALL baroclinicity timeseries ($r = 0.80$, $p < 0.05$). The WINDS sea-ice freshwater flux reproduces well the ALL sea-ice freshwater flux ($r = 0.94$, $p < 0.05$), especially preceding baroclinicity maxima (less sea-ice formation). The WINDS sea-ice freshwater flux preceding the 2016 baroclinicity minimum is, however, much weaker than in ALL. This is caused by the lack of atmospheric thermodynamic variability in WINDS, a factor which is more important during the opening of polynyas than during the closing of polynyas.

Past studies (O'Connor et al., 2025; St-Laurent et al., 2015; Webber et al., 2017) have suggested that heat fluxes in coastal polynyas drive variability in ice-shelf melting. We find that surface heat fluxes play a secondary role, evidenced by composites and timeseries of the surface heat flux (Figure S4 in Supporting Information S1) and the on-shelf heat budget (Figure S5 in Supporting Information S1). We conclude that wind-driven sea-ice freshwater fluxes explain most of the undercurrent and ice-shelf melt variability. The mechanism is summarized in Figure 5.

4. Discussion

We have considered natural decadal variability of ice-shelf melting, sea-ice melt/formation, and the undercurrent in the Amundsen Sea. On decadal timescales the undercurrent variability is baroclinic and opposes local wind variability (Haigh & Holland, 2024; Silvano et al., 2022). We have conducted a suite of perturbation experiments to determine the drivers of this baroclinic variability and resulting ice-shelf melt variability.

The undercurrent variability is driven by on-shelf density variability which alters the cross-slope baroclinic pressure gradient. The perturbation experiments reveal that the density variability is caused by the sea-ice freshwater flux variability in wind-driven coastal polynyas. With the perturbation experiments we also quantify a positive feedback mechanism between the undercurrent and ice-shelf melting, which is responsible for 25% of their decadal variability. A limitation of our model is that it uses climatological boundary conditions. While the model reproduces observed on-shelf thermocline variability (Figure S2 in Supporting Information S1), it has been shown that transient boundary conditions can have a secondary effect on modeled Amundsen Sea temperatures on

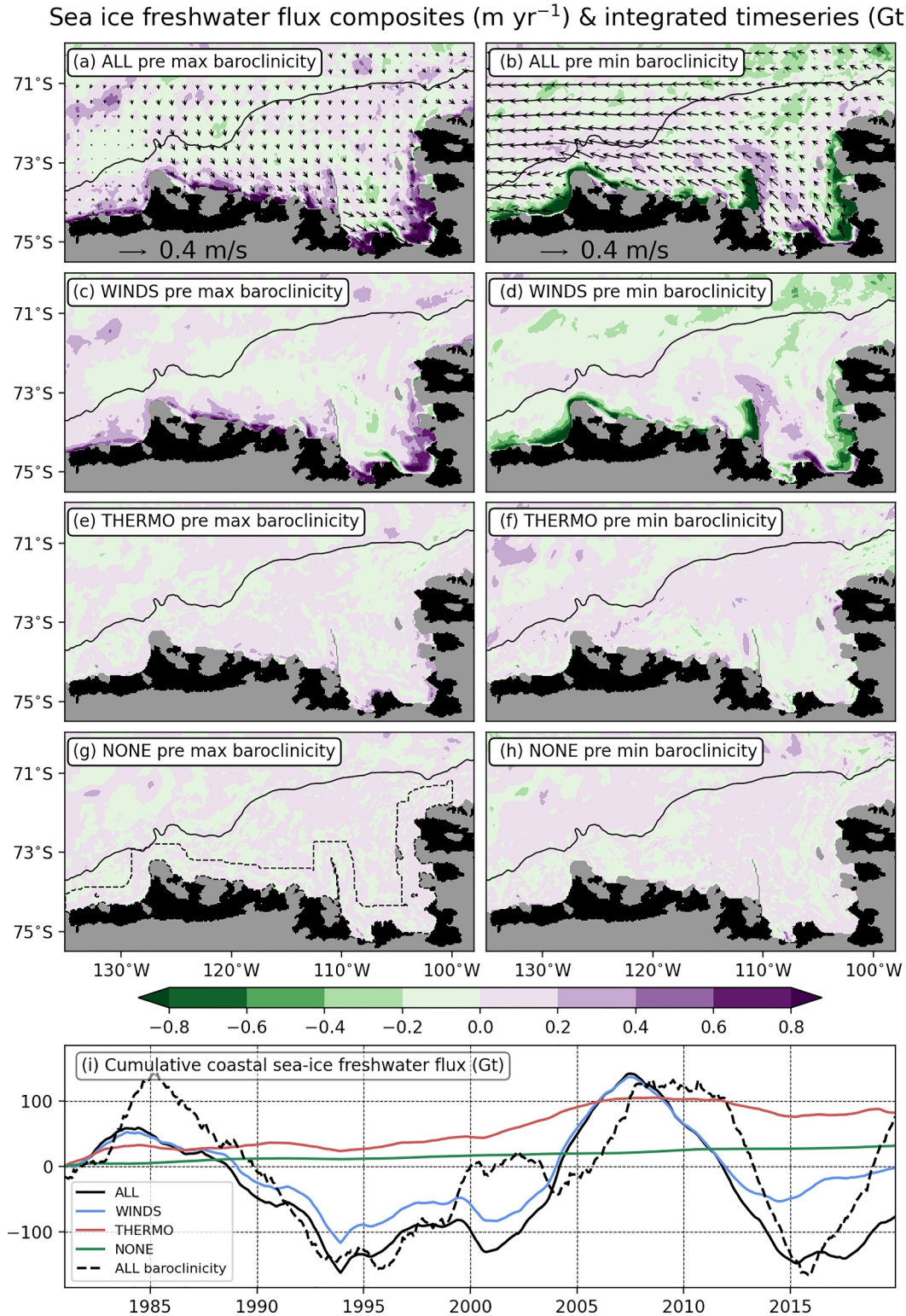

Figure 4. (a)–(h) Composites of the sea-ice freshwater flux anomaly averaged over periods preceding baroclinicity maxima and minima. Composites are for (a), (b) ALL (c), (d) WINDS (e), (f) THERMO and (g), (h) NONE. Panels (a), (b) also show composites of the winds. The black contour is the 1000 m shelf break isobath. (i) Time-integrated coastal sea-ice freshwater flux for ALL, WINDS, THERMO and NONE (coastal area of integration shown in (g)). The scaled ALL baroclinicity is also shown for comparison.

19448007, 2026, 2, Downloaded from https://agupubs.onlinelibrary.wiley.com/doi/10.1029/2025GL118546 by British Antarctic Survey, Wiley Online Library on [22/01/2026]. See the Terms and Conditions (https://onlinelibrary.wiley.com/terms-and-conditions) on Wiley Online Library for rules of use; OA articles are governed by the applicable Creative Commons License

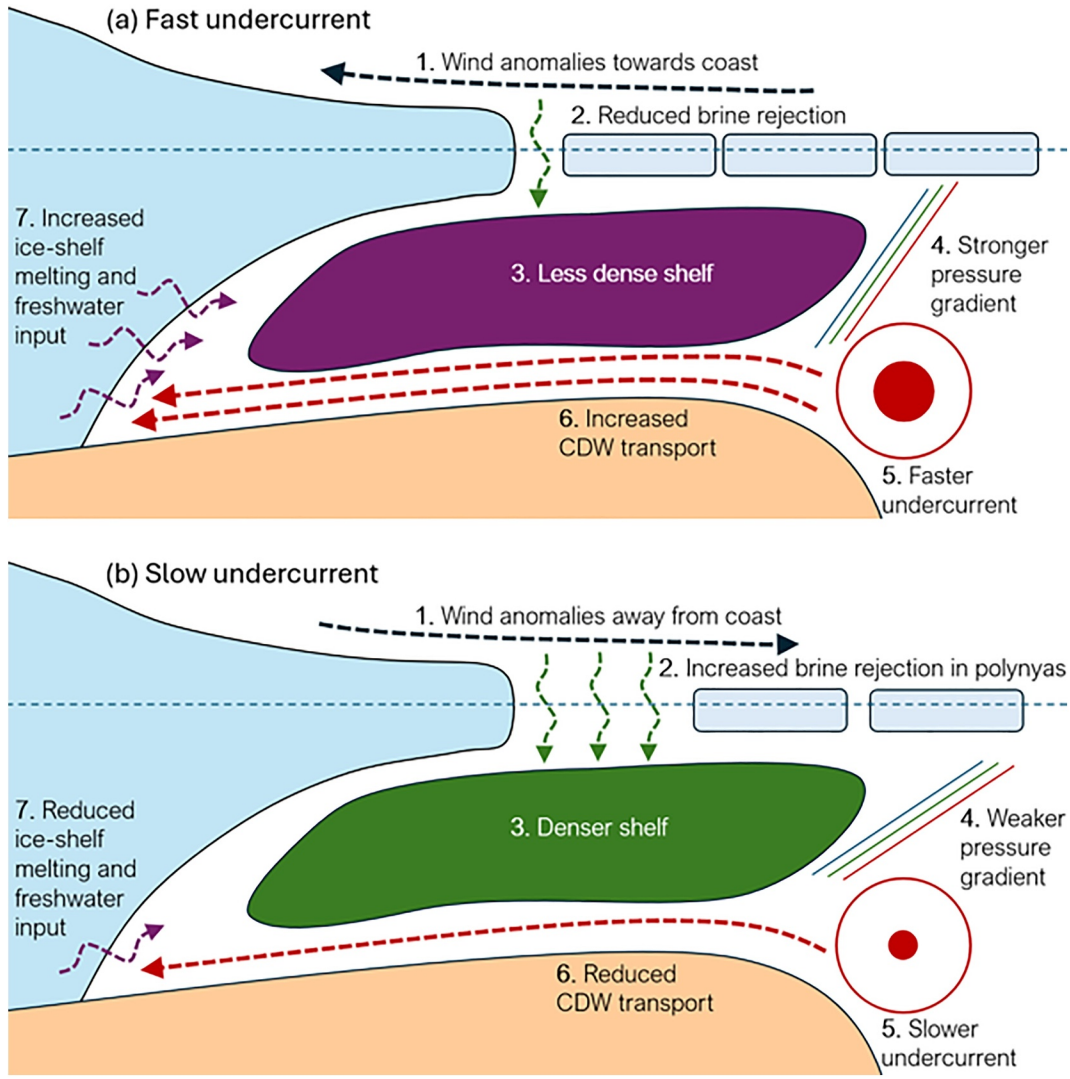

Figure 5. Schematic of the proposed mechanism. (a) Winds anomalies towards the coast lead to increased ice-shelf melting. (b) Wind anomalies away from the coast lead to reduced ice-shelf melting.

interannual timescales (Nakayama et al., 2018), and are essential when considering centennial timescales (Jourdain et al., 2022; Naughten et al., 2023).

Our results add to growing evidence that on longer timescales variability in the Amundsen Sea is controlled by buoyancy fluxes. Caillet et al. (2023) showed that wind stress variability can strongly affect sea-ice related buoyancy fluxes and in turn on-shelf temperature anomalies. Our study shows that the ice-shelf melt response to on-shelf temperature anomalies can augment itself via feedbacks with the undercurrent. Turner et al. (2025) showed that future trends in Amundsen Sea temperatures and ice-shelf melting are caused by reduced sea-ice formation. Finally, however, Jourdain et al. (2022) and Naughten et al. (2023) have both suggested that in a warmer future climate, the Amundsen Sea may no longer be sensitive to surface buoyancy fluxes. These conclusions underline the need for further research into future trends in ice-shelf melting in West Antarctica.

Conflict of Interest

The authors declare no conflicts of interest relevant to this study.

19448007, 2026, 2, Downloaded from https://agupubs.onlinelibrary.wiley.com/doi/10.1029/2025GL118546 by British Antarctic Survey, Wiley Online Library on [22/01/2026]. See the Terms and Conditions (https://onlinelibrary.wiley.com/terms-and-conditions) on Wiley Online Library for rules of use; OA articles are governed by the applicable Creative Commons License

Data Availability Statement

Subsetted model output and scripts for generating figures are available online (https://github.com/mhaigh/MITgcm_perturb). The MITgcm source code is publicly available (https://github.com/MITgcm/MITgcm) along with the specific configuration and edited source code used in this study (https://github.com/mhaigh/PAS_668).

Acknowledgments
This research was funded by the NERC project "Drivers of Oceanic Change in the Amundsen Sea", NE/T012803/1. The authors thank Kaitlin Naughten for providing edited MITgcm source code enabling separate output of sea ice freezing and melting components. The authors also thank David Bett for assistance with developing edits to the MITgcm shelfice package.

References

Assmann, K. M., Jenkins, A., Shoosmith, D. R., Walker, D. P., Jacobs, S. S., & Nicholls, K. W. (2013). Variability of circumpolar deep water transport onto the Amundsen Sea Continental shelf through a shelf break trough. *Journal of Geophysical Research: Oceans*, *118*(12), 6603–6620. https://doi.org/10.1002/2013jc008871

Azaneu, M., Webber, B., Heywood, K. J., Assmann, K. M., Dotto, T. S., & Abrahamsen, E. P. (2023). Influence of shelf break processes on the transport of warm waters onto the eastern Amundsen Sea Continental shelf. *Journal of Geophysical Research: Oceans*, *128*(5), e2022JC019535. https://doi.org/10.1029/2022JC019535

Caillet, J., Jourdain, N. C., Mathiot, P., Hellmer, H. H., & Mouginot, J. (2023). Drivers and reversibility of abrupt ocean state transitions in the Amundsen Sea, Antarctica. *Journal of Geophysical Research: Oceans*, *128*(1), e2022JC018929. https://doi.org/10.1029/2022jc018929

Dotto, T. S., Naveira Garabato, A. C., Bacon, S., Holland, P. R., Kimura, S., Firing, Y. L., et al. (2019). Wind-driven processes controlling Oceanic heat delivery to the Amundsen Sea, Antarctica. *Journal of Physical Oceanography*, *49*(11), 2829–2849. https://doi.org/10.1175/jpo-d-19-0064.1

Dotto, T. S., Naveira Garabato, A. C., Wåhlin, A. K., Bacon, S., Holland, P. R., Kimura, S., & Jenkins, A. (2020). Control of the Oceanic heat content of the getz-dotson trough, Antarctica, by the Amundsen Sea low. *Journal of Geophysical Research: Oceans*, *125*(8), e2020JC016113. https://doi.org/10.1029/2020jc016113

Dutrieux, P., Rydt, J. D., Jenkins, A., Holland, P. R., Ha, H. K., Lee, S. H., et al. (2014). Strong sensitivity of pine island ice-shelf melting to climatic variability. *Science*, *343*(6167), 174–178. https://doi.org/10.1126/science.1244341

Gossart, A., Helsen, S., Lenaerts, J. T. M., Broucke, S. V., van Lipzig, N. P. M., & Souverijns, N. (2019). An evaluation of surface climatology in state-of-the-art reanalyses over the Antarctic ice sheet. *Journal of Climate*, *32*(20), 6899–6915. https://doi.org/10.1175/JCLI-D-19-0030.1

Haigh, M., & Holland, P. R. (2024). Decadal variability of ice-shelf melting in the Amundsen Sea driven by sea-ice freshwater fluxes. *Geophysical Research Letters*, *51*(9), e2024GL108406. https://doi.org/10.1029/2024GL108406

Haigh, M., Holland, P. R., & Jenkins, A. (2023). The influence of bathymetry over heat transport onto the Amundsen Sea Continental shelf. *Journal of Geophysical Research: Oceans*, *128*(5), e2022JC019460. https://doi.org/10.1029/2022jc019460

Hersbach, H., Bell, B., Berrisford, P., Hirahara, S., Horányi, A., Muñoz-Sabater, J., et al. (2020). The ERA5 global reanalysis. *Quarterly Journal of the Royal Meteorological Society*, *146*(730), 1999–2049. https://doi.org/10.1002/qj.3803

Holland, P. R., Bracegirdle, T. J., Dutrieux, P., Jenkins, A., & Steig, E. J. (2019). West Antarctic ice loss influenced by internal climate variability and anthropogenic forcing. *Nature Geoscience*, *12*(9), 718–724. https://doi.org/10.1038/s41561-019-0420-9

Jenkins, A., Dutrieux, P., Jacobs, S., Steig, E., Gudmundsson, H., Smith, J., & Heywood, K. (2016). Decadal ocean forcing and Antarctic ice sheet response: Lessons from the Amundsen Sea. *Oceanography*, *29*(4), 106–117. https://doi.org/10.5670/oceanog.2016.103

Jenkins, A., Shoosmith, D., Dutrieux, P., Jacobs, S., Kim, T. W., Lee, S. H., et al. (2018). West Antarctic ice sheet retreat in the Amundsen Sea driven by decadal Oceanic variability. *Nature Geoscience*, *11*(10), 733–738. https://doi.org/10.1038/s41561-018-0207-4

Jourdain, N. C., Mathiot, P., Burgard, C., Caillet, J., & Kittel, C. (2022). Ice shelf basal melt rates in the Amundsen Sea at the end of the 21st century. *Geophysical Research Letters*, *49*(22), e2022GL100629. https://doi.org/10.1029/2022gl100629

Macdonald, G. J., Ackley, S. F., Mestas-Nuñez, A. M., & Blanco-Cabanillas, A. (2023). Evolution of the dynamics, area, and ice production of the Amundsen Sea polynya, Antarctica, 2016–2021. *The Cryosphere*, *17*(2), 457–476. https://doi.org/10.5194/tc-17-457-2023

Moorman, R., Morrison, A. K., & McC. Hogg, A. (2020). Thermal responses to Antarctic ice shelf melt in an eddy-rich global ocean–sea ice model. *Journal of Climate*, *33*(15), 6599–6620. https://doi.org/10.1175/jcli-d-19-0846.1

Mouginot, J., Rignot, E., & Scheuchl, B. (2014). Sustained increase in ice discharge from the Amundsen Sea embayment, west Antarctica, from 1973 to 2013. *Geophysical Research Letters*, *41*(5), 1576–1584. https://doi.org/10.1002/2013gl059069

Nakata, K., Ohshima, K. I., & Nihashi, S. (2021). Mapping of active frazil for antarctic coastal polynyas, with an estimation of sea-ice production. *Geophysical Research Letters*, *48*(6), e2020GL091353. https://doi.org/10.1029/2020GL091353

Nakayama, Y., Menemenlis, D., Zhang, H., Schodlok, M., & Rignot, E. (2018). Origin of circumpolar deep water intruding onto the Amundsen and bellingshausen sea Continental shelves. *Nature Communications*, *9*(1), 3403. https://doi.org/10.1038/s41467-018-05813-1

Naughten, K. A., Holland, P. R., & De Rydt, J. (2023). Unavoidable future increase in west Antarctic ice-shelf melting over the twenty-first century. *Nature Climate Change*, *13*(11), 1222–1228. https://doi.org/10.1038/s41558-023-01818-x

Naughten, K. A., Holland, P. R., Dutrieux, P., Kimura, S., Bett, D. T., & Jenkins, A. (2022). Simulated twentieth-century ocean warming in the Amundsen Sea, west Antarctica. *Geophysical Research Letters*, *49*(5), e2021GL094566. https://doi.org/10.1029/2021gl094566

O'Connor, G., Nakayama, Y., Steig, E., Armour, K., Thompson, L., Hyogo, S., et al. (2025). Enhanced west antarctic ice loss triggered by polynya response to meridional winds. *Nature Geoscience*.

Rignot, E., Mouginot, J., Morlighem, M., Seroussi, H., & Scheuchl, B. (2014). Widespread, rapid grounding line retreat of pine island, Thwaites, smith, and kohler glaciers, west Antarctica, from 1992 to 2011. *Geophysical Research Letters*, *41*(10), 3502–3509. https://doi.org/10.1002/2014gl060140

Shepherd, A., Ivins, E., Rignot, E., Smith, B., van den Broeke, M., Velicogna, I., & others (2018). Mass balance of the Antarctic ice sheet from 1992 to 2017. *Nature*, *558*(7709), 219–222. https://doi.org/10.1038/s41586-018-0179-y

Si, Y., Stewart, A. L., & Eisenman, I. (2023). Heat transport across the Antarctic slope front controlled by cross-slope salinity gradients. *Science Advances*, *9*(18), eadd7049. https://doi.org/10.1126/sciadv.add7049

Silvano, A., Holland, P. R., Naughten, K. A., Dragomir, O., Dutrieux, P., Jenkins, A., et al. (2022). Baroclinic ocean response to climate forcing regulates decadal variability of ice-shelf melting in the Amundsen Sea. *Geophysical Research Letters*, *49*(24), e2022GL100646. https://doi.org/10.1029/2022gl100646

Stewart, K., Kim, W., Urakawa, S., Hogg, A., Yeager, S., Tsujino, H., et al. (2020). JRA55-do-based repeat year forcing datasets for driving ocean–sea-ice models. *Ocean Modelling*, *147*, 101557. https://doi.org/10.1016/j.ocemod.2019.101557

St-Laurent, P., Klinck, J. M., & Dinniman, M. S. (2015). Impact of local winter cooling on the melt of pine island glacier, Antarctica. *Journal of Geophysical Research: Oceans*, *120*(10), 6718–6732. https://doi.org/10.1002/2015jc010709

19448007, 2026, 2, Downloaded from https://agupubs.onlinelibrary.wiley.com/doi/10.1029/2025GL118546 by British Antarctic Survey, Wiley Online Library on [22/01/2026]. See the Terms and Conditions (https://onlinelibrary.wiley.com/terms-and-conditions) on Wiley Online Library for rules of use; OA articles are governed by the applicable Creative Commons License

Tetzner, D., Thomas, E., & Allen, C. (2019). A validation of ERA5 reanalysis data in the southern Antarctic peninsula—Ellsworth land region, and its implications for ice core studies. *Geosciences*, *9*(7), 289. https://doi.org/10.3390/geosciences9070289

Turner, K. A., Naughten, K. A., Holland, P. R., & Naveira Garabato, A. C. (2025). Modeled Centennial ocean warming in the Amundsen Sea driven by thermodynamic atmospheric changes, not winds. *Geophysical Research Letters*, *52*(14), e2024GL112287. https://doi.org/10.1029/2024GL112287

Walker, D. P., Brandon, M. A., Jenkins, A., Allen, J. T., Dowdeswell, J. A., & Evans, J. (2007). Oceanic heat transport onto the Amundsen Sea shelf through a submarine glacial trough. *Geophysical Research Letters*, *34*(2), L02602. https://doi.org/10.1029/2006gl028154

Walker, D. P., Jenkins, A., Assmann, K. M., Shoosmith, D. R., & Brandon, M. A. (2013). Oceanographic observations at the shelf break of the Amundsen Sea, Antarctica. *Journal of Geophysical Research: Oceans*, *118*(6), 2906–2918. https://doi.org/10.1002/jgrc.20212

Webber, B. G. M., Heywood, K. J., Stevens, D. P., Dutrieux, P., Abrahamsen, E. P., Jenkins, A., et al. (2017). Mechanisms driving variability in the ocean forcing of pine island Glacier. *Nature Communications*, *8*(1), 14507. https://doi.org/10.1038/ncomms14507

References From the Supporting Information

Bett, D. T., Holland, P. R., Naveira Garabato, A. C., Jenkins, A., Dutrieux, P., Kimura, S., & Fleming, A. (2020). The impact of the Amundsen Sea freshwater balance on Ocean melting of the west Antarctic ice sheet. *Journal of Geophysical Research: Oceans*, *125*(9), e2020JC016305. https://doi.org/10.1029/2020jc016305

Jacobs, S. S., Hellmer, H. H., & Jenkins, A. (1996). Antarctic ice sheet melting in the southeast Pacific. *Geophysical Research Letters*, *23*(9), 957–960. https://doi.org/10.1029/96GL00723

Locarnini, R. A., Mishonov, A. V., Antonov, J. I., Boyer, T. P., Garcia, H. E., Baranova, O. K., & Seidov, D. (2013). *World ocean atlas 2013*, Vol. 1. Temperature. https://doi.org/10.7289/V55X26VD

Nakata, K., Ohshima, K. I., & Nihashi, S. (2019). Estimation of thin-ice thickness and discrimination of ice type from AMSR-E passive microwave data. *IEEE Transactions on Geoscience and Remote Sensing*, *57*(1), 263–276. https://doi.org/10.1109/TGRS.2018.2853590

Verdy, A., & Mazloff, M. R. (2017). A data assimilating model for estimating Southern Ocean biogeochemistry. *Journal of Geophysical Research: Oceans*, *122*(9), 6968–6988. https://doi.org/10.1002/2016JC012650

Zhou, S., Dutrieux, P., Giulivi, C., Lee, W. S., Kim, T.-W., Hattermann, T., & Janout, M. (2024). Southern Ocean (90°S-45°S) conservative temperature and absolute salinity profiles compilation (OCEAN ICE D1.1) [Dataset]. https://doi.org/10.17882/99787

Zhou, S., Dutrieux, P., Giulivi, C. F., Jenkins, A., Silvano, A., Auckland, C., et al. (2025). The OCEAN ICE mooring compilation: A standardised, pan-Antarctic database of ocean hydrography and current time series. *Earth System Science Data*, *17*(10), 5693–5706. https://doi.org/10.5194/essd-17-5693-2025

19448007, 2026, 2, Downloaded from https://agupubs.onlinelibrary.wiley.com/doi/10.1029/2025GL118546 by British Antarctic Survey, Wiley Online Library on [22/01/2026]. See the Terms and Conditions (https://onlinelibrary.wiley.com/terms-and-conditions) on Wiley Online Library for rules of use; OA articles are governed by the applicable Creative Commons License